Charge-Transfer-Induced Insulator−Superconductor Transition in $TlBa_{2-x}Sr_xCa_{0.4}Pr_{0.6}Cu_2O_{7-\delta}$: A Joint Neutron/X-ray Rietveld Refinement, Infrared Absorption, and Raman Scattering Studies

A. Sundaresan, C. Michel,* and B. Raveau

Laboratoire CRISMAT, ISMRA, 6 Bd du Maréchal Juin 14050, Caen, France

P. V. Huong

Laboratoire de Spectroscopie Moleculaire et Cristalline, Universite Bordeaux I, 351 Cours Liberation, 33405 Talence, France

Received May 20, 1997. Revised Manuscript Received August 4, 1997[⊗]

Insulator-superconductor transition in $TlBa_{2-x}Sr_xCa_{0.4}Pr_{0.6}Cu_2O_{7-\delta}$ has been investigated by a joint Rietveld refinement of neutron and X-ray diffraction data, Raman scattering, and infrared absorption studies. For $x = 0$, the system is an insulator. Substitution of the Ba^{2+} ions by smaller Sr^{2+} ions leads to a transition from semiconductor to metal then superconductor for $x = 1.0$. Further, the superconducting transition temperature (T_c) increases with x. Results of the joint neutron/X-ray Rietveld refinement revealed that the Tl−O(1) apical bond length does not change appreciably while the Cu−O(1) bond length decreases largely when x increases, consistent with an electron transfer from Cu to Tl. This idea is supported by the Raman scattering measurements showing a large frequency shift of the phonon mode involving the motion of O(1) toward Tl, when Ba is replaced by Sr.

1. Introduction

In $Tl_2A_2Ca_{n-1}Cu_nO_{2n+4}$ (Tl-2) superconductors, where A = Ba, Sr, it has been suggested[1−5] that the holes in the CuO_2 layers could be generated by charge transfer or oxidation−reduction (redox) mechanism $Tl^{3+} + Cu^{2+} \leftrightarrow Tl^{3-\delta} + Cu^{2+\delta}$. The $TlA_2Ca_{n-1}Cu_nO_{2n+3}$ (Tl-1) compounds, according to the stoichiometric formula, have higher hole concentration which is in agreement with the fact that these materials are in overdoped state.[6,7] This is the main reason that they are difficult to prepare as a single phase. However, they can be stabilized, for example, by the substitution of divalent Ba^{2+}, Sr^{2+}, and Ca^{2+} ions by trivalent rare earths. Although the Ba- and Sr-based Tl-1 ($n = 1$ and 2) compounds have the same tetragonal structure (space group $P4/mmm$), for a given n and rare earth, they differ from each other in the following. The Ba-based Tl-1 compounds can be stabilized and the maximum T_c can be obtained with a lower concentration of rare earths than that required for Sr-based Tl-1 compounds. This seems to indicate that the Sr-based $TlSr_2Ca_{n-1}Cu_nO_{2n+3}$ ($n = 1$ and 2) compounds contain higher hole concentration than that in the Ba-based $TlBa_2Ca_{n-1}Cu_nO_{2n+3}$ compounds.

In the case of the first ($n = 1$) member of Sr-based Tl-1 system, experiments, and band electronic structure calculations suggest the presence of a charge transfer or redox mechanism of generation of holes as suggested for the Tl-2 compounds.[8−11] In the case of the second member ($n = 2$), the superconducting behavior and XPS measurements did indicate that the redox mechanism may also be operating.[12] However, a systematic study of this member is required to understand various mechanisms for a generation of holes which are responsible for the difference in the behavior of the superconducting properties. For this purpose, we have investigated a system, $TlBa_{2-x}Sr_xCa_{0.4}Pr_{0.6}Cu_2O_{7-\delta}$ by a joint neutron/X-ray Rietveld refinement, Raman scattering, and infrared absorption measurements. Our study shows that this system undergoes a transition from semiconductor to superconductor upon substitution of Ba^{2+} for smaller Sr^{2+} ions. Large shift of the frequency of the apical oxygen vibration in the absence of significant change in the corresponding bond length suggests the charge transfer from Tl ions to CuO_2 layers which could be considered to be responsible for the semiconductor−superconductor transition observed in $TlBa_{2-x}Sr_xCa_{0.4}Pr_{0.6}Cu_2O_{7-\delta}$.

2. Experiments and Results

The samples $TlBa_{2-x}Sr_xCa_{0.4}Pr_{0.6}Cu_2O_{7-\delta}$ ($x = 0.0$, 0.5, 1.0, 1.5, and 2.0) of 8 g each were prepared by the

[⊗] Abstract published in *Advance ACS Abstracts,* September 15, 1997.

(1) Matthaiss, L. F.; Hamann, D. R. *Phys. Rev. B* **1988**, *38*, 5012.
(2) Jung, D.; Whanghbo, M. H.; Herron, N.; Torardi, C. *Physica C* **1989**, *160*, 381.
(3) Suzuki, T.; Nogoshi, M.; Fukuda, Y.; Nakajima, S.; Kikuchi, M.; Syono, Y.; Tachiki, M. *Phys. Rev. B* **1989**, *40*, 5184.
(4) Meyer, H. M.; Wagener, T. J.; Weaver, J. H. *Phys. Rev. B* **1989**, *39*, 7343.
(5) Raveau, B.; Martin, C.; Provost, J.; Hervieu, M. *Solid State Ionics* **1990**, *40/41*, 785.
(6) Martin, C.; Maignan, A.; Provost, J.; Michel, C.; Hervieu, M. *Physica C* **1990**, *168*, 8.
(7) Nakajima, S.; Kikuchi, M.; Syono, Y.; Kobayashi, N. *Physica C* **1991**, *185−189*, 673.
(8) Whangbo, M. H.; Subramanian, M. A. *J. Solid State Chem.* **1991**, *91*, 403.
(9) Sundaresan, A.; Gopinath, C. S.; Tamhane, A. S.; Rajarajan, A. K.; Sharon, M.; Subramanyan, S.; Pinot, R.; Gupta, L. C.; Vijayaraghavan, R. *Phys. Rev. B* **1992**, *46*, 6622.
(10) Mertelj, T.; Sundaresan, A.; Gupta, L. C.; Sharon, M.; Mihailovic, D. *Solid State Commun.* **1993**, *88*, 271.
(11) Sharma, R.; Sundaresan, A.; Sequeira, A.; Sharon, M.; Gupta, L. C. *Phys. Rev. B* **1995**, *52*, 4427.
(12) Sundaresan, A.; Gopinath, C. S.; Subramanyan, S.; Gupta, L. C.; Sharon, M.; Vijayaraghavan, R. *Phys. Rev. B* **1994**, *50*, 10238.

S0897-4756(97)00377-3 CCC: $14.00 © 1997 American Chemical Society

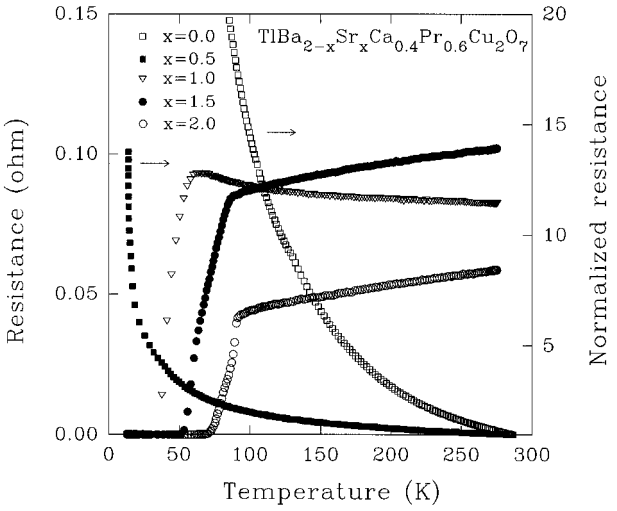

Figure 1. Semiconductor−superconductor transition in $TlBa_{2-x}Sr_xCa_{0.4}Pr_{0.6}Cu_2O_{7-\delta}$.

standard solid-state reaction method in a sealed silica tube using the starting materials Tl_2O_3, BaO_2, Sr_2CuO_3, CaO, Pr_6O_{11}, and CuO. The reaction temperature was 900 °C. To avoid explosion of a silica tube containing an oxygen generator (BaO_2) which will generate pressure in the tube at the reaction temperature, the samples were prepared in 1 g batches. Then the product from the different batches were mixed together and annealed in oxygen flow at 850 °C for 15 min and cooled in the furnace to room temperature. Phase purity was checked by an X-ray Guinier pattern. High-resolution powder X-ray data were collected by steps of 0.02° in the 2θ range 5−120° with a Philips diffractometer. Room-temperature neutron diffraction data were collected for the samples with $x = 0.0$, 1.0 and 2.0 at the ILL, Grenoble, on the diffractometer D1A ($\lambda = 1.909$ Å) in the 2θ range 0−160°. Resisitivity measurements were carried out by the standard four-probe method.

Room-temperature Raman spectra on various scattering geometries have been recorded on a Raman microspectrometer DILOR Model OMARS equipped with a CCD detector and an argon laser source Spectra Physics 2017 emiting at 5.145 nm. The spatial resolution is around 1 μm^2.[13−15] The laser power was kept always lower than 20 mW to avoid any damage or photoinduction. The spectra were recorded on microcrystals of about 1−10 μm of different samples used for neutron diffraction and other studies. Since the microcrystals are selected from polycrystalline materials, the crystals were not perfectly oriented. As a consequence, the various polarization of Raman spectra could not be assigned accurately. Infrared absorption measurement were made at room temperature with a Nicolet Magna 750 Fourier transform instrument.

Powder X-ray diffraction pattern showed that the samples are nearly single phase with the tetragonal structure (space group *P*4/*mmm*) and indicated the presence of small amount of carbonate impurities. Trace of unidentified impurity phase was noticed from the neutron data. The results of the resistivity measurements are shown in Figure 1. It can be seen that the $\rho(T)$ for the sample with $x = 0$, having 0.2 hole/copper according to the formula with $\delta \sim 0$, shows a semiconducting behavior. With increasing x it undergoes a semiconductor to metal transition then superconductor at low temperatures. The superconducting transition temperature (T_c) increases with x. This behavior indicates that in the sample with $x = 0$ the holes are localized or the sample is underdoped. Furthermore, with increasing x, the holes become delocalized due to the chemical pressure induced by the substitution of Ba^{2+} by smaller Sr^{2+} ions or the hole concentration is increased by the charge transfer or redox mechanism.

A. Joint Neutron/X-ray Rietveld Refinement. Neutron and high-resolution X-ray diffraction data were collected only for three samples with $x = 0$, 1.0, and 2.0 and analyzed by Rietveld refinement using the program General Structure Analysis System (GSAS).[16] Initially the neutron data alone were analyzed using the neutron scattering length for various atoms as given in the GSAS package. The initial atomic positions were those reported for the isostructural $TlBa_2Ca_{1-x}Nd_xCu_2O_7$ system.[17] Carbonate impurity phases were also included at a later stage of refinement. First, the profile parameters such as scale factor, background polynomial coefficients, zero shift, peak-shape, and lattice parameters were refined. Then the atomic parameters, positional and isotropic thermal displacements (U_{iso}), were refined. Such a refinement led to a fairly good profile fit. But the U_{iso} values for Tl and oxygen in the Tl−O plane O(3) were quite high. Analysis of difference Fourier maps revealed that the Tl and O(3) atoms were displaced from the ideal (0, 0, 0) and (0.5, 0.5, 0) positions to disorderd (0, y, 0) and (0.5, y, 0) positions, respectively. This behavior is commonly observed in many Tl-based systems and has been attributed to short-range ordering in the Tl−O(3) plane. Therefore, the Tl and O(3) positions were refined according to the disordered positions. Such a refinement resulted in reasonable U_{iso} and R_P values. However, the U_{iso} for Ca/Pr was found to be close to zero or negative. Also attempt to refine their ratio leads to indiscriminate value. This may be due to similarity in neutron scattering length for Ca and Pr.

To obtain complete structural parameters with high accuracy, a joint neutron and X-ray Rietveld refinement was carried out. This strategy of joint refinement provides sensitivity to Ca/Pr (X-ray data) while maintaining a good accuracy to oxygen positions, occupancy, and thermal motions (neutron data). Similar joint Rietveld refinement allowed to establish the Mo distribution at the Cu site in $HoSr_2Cu_{2.7}Mo_{0.3}O_{7.54}$ where Mo and Cu have similar neutron scattering lengths.[18]

After the inclusion of the X-ray data, the refinement gave reasonable values for isotropic thermal parameters for Ca/Pr. Then the ratio of Ca/Pr was refined with the constraint that the total occupancy (N) was one. Finally, we attempted to refine the thermal parameters as anisotropic. Although the refinement gave a good anisotropic thermal displacement value for most of the

(13) Huong, P. V. *Studies of High Temperature Superconductors*; Narlikar, Ed.; Nova Science: New York, 1995; Vol. 13.
(14) Huong, P. V.; Verma, A. L. *Phys. Rev. B* **1993**, *48*, 9869.
(15) Huong, P. V. *Fresenius J. Anal. Chem.* **1996**, *355*, 596.
(16) Larson, A. C.; Von Dreele, R. B. *GSAS User Guide, Los Alamos National Laboratory*; 1990.
(17) Michel, C.; Suard, E.; Caignaert, V.; Martin, C.; Maignan, A.; Hervieu, M.; Raveau, B. *Physica C* **1991**, *178*, 29.
(18) Harrison, W. T. A.; Roliard, S.; Vaughey, J. T.; Liu, L.; Jacobson, A. J. *J. Solid State Chem.* **1995**, *119*, 115.

Table 1. Positional and Thermal Parameters for $TlBa_{2-x}Sr_xCa_{0.4}Pr_{0.6}Cu_2O_{7-\delta}$ with $x = 0$, 1.0, and 2.0 Obtained from a Joint Neutron/X-ray Rietveld Refinement with the Space Group *P4/mmm*[a]

	x		
	0.0	1.0	2.0
a (Å)	3.88416(3)	3.85262(4)	3.82620(8)
c (Å)	12.5430(2)	12.2813(2)	12.1262(3)
Tl (4*l*) 0,*y*,0			
y	0.0843(8)	0.080(1)	0.073(1)
U_{iso}	0.80(9)	0.6(1)	0.40(1)
N	0.25	0.241(1)	0.235(1)
Ba/Sr (2*h*) $^1/_2,^1/_2,z$			
z	0.2103(1)	0.2094(1)	0.2101(1)
U_{iso}	0.67(4)	1.13(6)	0.99(6)
Ca/Pr (1*d*) $^1/_2,^1/_2,^1/_2$			
U_{iso}	0.40(7)	0.21(8)	0.22(8)
N	0.424(7)/ 0.576(7)	0.432(6)/ 0.568(6)	0.48(5)/ 0.52(5)
Cu (2*g*) 0,0,*z*			
z	0.3675(1)	0.3621(1)	0.3580(1)
U_{iso}	0.44(4)	0.91(5)	0.87(6)
O1 (2*g*) 0,0,*z*			
z	0.1644(2)	0.1681(2)	0.1697(3)
U_{iso}	1.49(5)	2.19(7)	1.57(7)
O2 (4*i*) $^1/_2$,0,*z*			
z	0.3790(1)	0.3742(1)	0.3693(2)
U_{iso}	0.87(4)	1.23(5)	1.08(5)
O3 (4*n*) $^1/_2$,*y*,0			
y	0.395(1)	0.399(2)	0.402(2)
U_{iso}	1.2(2)	2.2(3)	0.4(3)
N	0.25	0.245(4)	0.240(4)
R_P	6.85%	6.97%	6.01%
R_{WP}	8.96%	8.92%	8.77%
χ^2	4.12	4.23	3.60

[a] Figures in the parentheses represent the esd's referred to the last digits. Thermal parameters are multiplied by 100, and the units are Å^2.

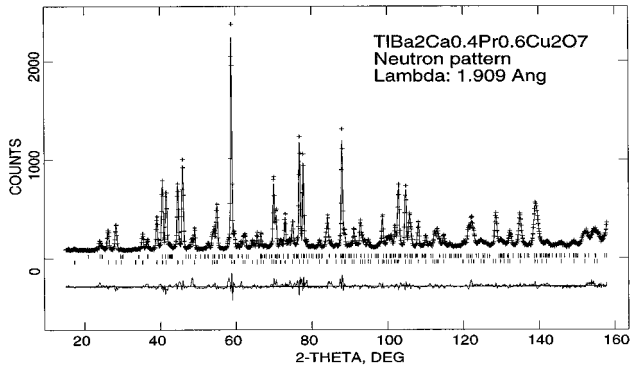

Figure 2. Observed (plus marks), calculated (continuous line), and difference neutron profile for $TlBa_2Ca_{0.4}Pr_{0.6}Cu_2O_7$. Allowed reflection positions for the main (top) and the impurity $BaCO_3$ phases are marked by vertical tick marks.

atoms, the agreement factors did not improve much. Also, for a few atoms the thermal parameters were found to be close to zero or negative. This may be due to a low *Q* range for the neutron data. Therefore, we decided to restrict the thermal displacement of all the atoms as isotropic. The agreement and the structural parameters at convergence for all the samples are given in Table 1. The final neutron and X-ray profiles for the sample with $x = 0$ is shown in Figures 2 and 3, respectively. Various bond lengths obtained from the refinement are given in Table 2. The structure of Tl-$(Ba,Sr)_2Ca_{0.4}Pr_{0.6}Cu_2O_7$ is shown in Figure 4 where, for the sake of simplicity, the Tl and O(3) atoms are shown to occupy their ideal positions.

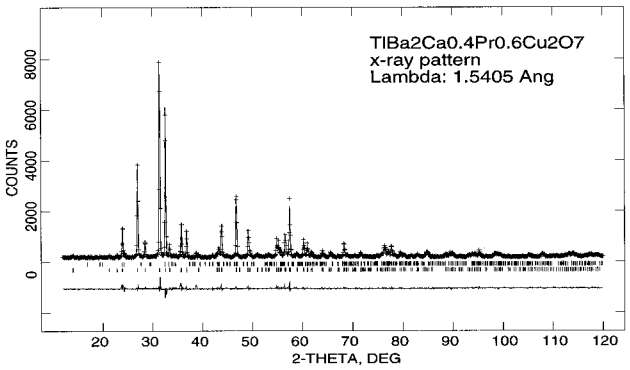

Figure 3. Observed (plus marks), calculated (continuous line), and difference X-ray profile for $TlBa_2Ca_{0.4}Pr_{0.6}Cu_2O_7$. Allowed reflection positions for the main (top) and the impurity $BaCo_3$ phases are marked by vertical tick marks.

Table 2. Selected Bond Lengths and Angles Obtained from the Joint Rietveld Refinement[a]

	x		
various bonds	0	1.0	2.0
Tl−O(1) × 2	2.087(2)	2.087(3)	2.076(3)
Tl−O(3) × 4	2.226(4)− 2.853(5)	2.231(6)− 2.825(6)	2.245(6)− 2.811(6)
Ba/Sr−O(3) × 4	2.670(2)	2.602(2)	2.574(2)
Ba/Sr−O(2) × 4	2.872(1)	2.794(1)	2.718(2)
Ba/Sr−O(1) × 4	2.8063(5)	2.7711(5)	2.7494(6)
Ca/Pr−O(2) × 8	2.4647(8)	2.470(1)	2.485(1)
Cu−O(1) × 1	2.548(3)	2.383(3)	2.283(4)
Cu−O(2) × 2	1.9474(2)	1.9320(2)	1.9180(2)
O(2)−Cu-O(2)	171.5(1)	171.1(1)	171.8(2)
Cu−Cu	3.273	3.3413	3.4082

[a] Units for the bond length Å.

It can be seen from Table 1 that only the Sr-containing samples show a small deficiency of thallium. This may be due to smaller oxygen pressure maintained during the synthesis than that for a full Ba-containing sample. The deficiency of Tl is in agreement with our EDX analysis. In the case of a full Ba sample, since the refinement gave a slight excess of Tl occupancy, the occupancy of Tl was fixed to 1.0. The observed excess of occupancy may be due to the presence of traces of unidentified impurity phase present in the sample. There is a small deficiency of oxygen in the Tl−O plane in the Sr-containing samples. For a full Ba sample, it was fixed to 1.0. The refined value of the ratio of Ca/Pr shows a small increase with *x*.

B. Infrared Absorption. According to group theory, the irreducible representations of the optical phonons at the Brillouin zone for Tl-1212 system are $4A_{1g} + B_{1g} + 5E_g$ and $7A_{2u} + B_{2u} + 8E_u$ for the Raman and infrared-active modes, respectively. The midinfrared (MIR) spectra for five samples ($x = 0.0$, 0.5, 1.0, 1.5, and 2.0) are shown in Figure 5a. The features around 2300 and 667 cm^{-1} are due to CO_2 present in the spectrometer atmosphere. The features at around 1600 and 3500 cm^{-1} represent H_2O, while the features at 1450 and 850 cm^{-1} are due to vibrational modes of carbonate impurities present in the sample. The features between 640 and 400 cm^{-1} are intrinsic to the sample. This is shown in Figure 5b in an expanded energy scale.

It can be seen that the MIR background increases with an increase of *x*, which is consistent with the appearance of metallicity. Only two phonon modes are observed at 559 and 433 cm^{-1} for $x = 0$. Also there is

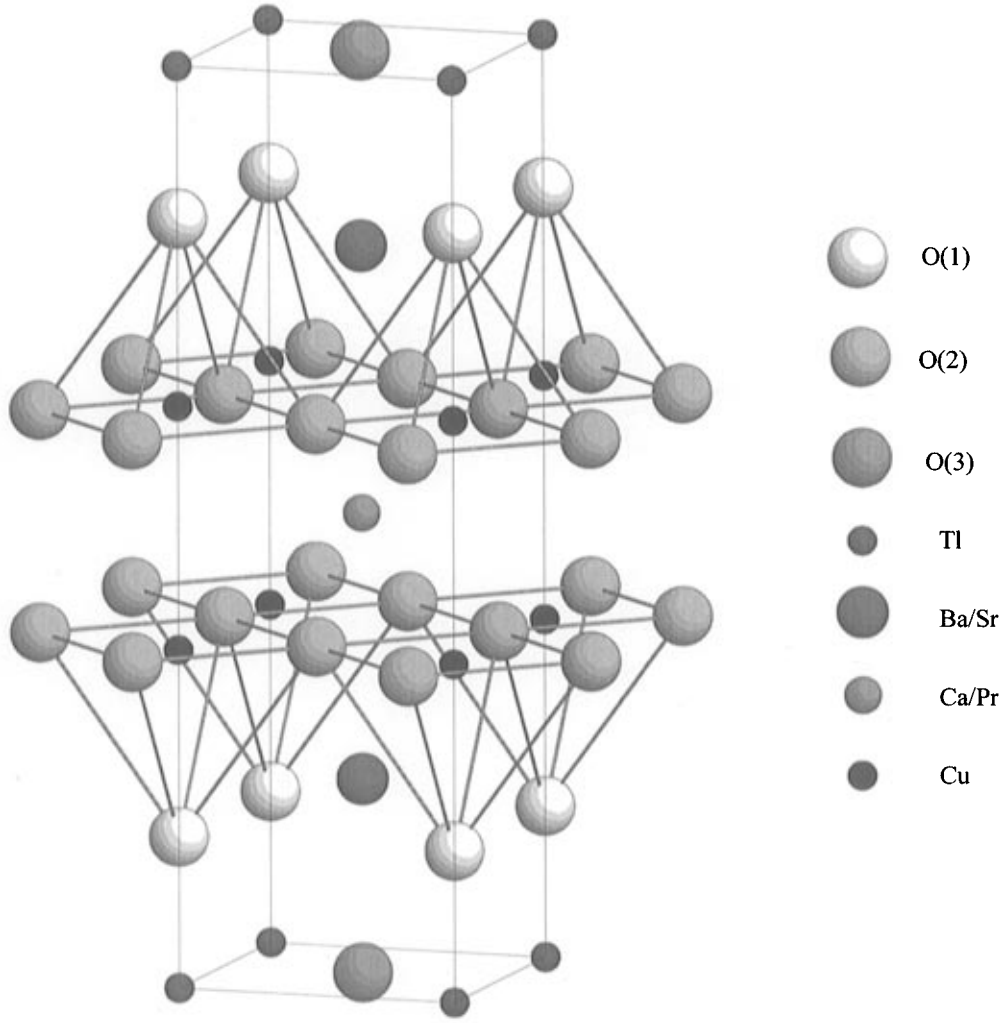

Figure 4. Crystal structure of $Tl(Ba,Sr)_2Ca_{0.4}Pr_{0.6}Cu_2O_7$. Disordering of Tl and O(3) atoms are not shown here.

a weak feature around 620 cm^{-1}. This is seen only in the semiconducting samples. By comparison with the lattice dynamical calculations,[10,20] we attribute this to an E_u mode which involves stretching vibration of O(2) in the CuO_2 layer. Its intensity for $x = 0$ is so weak may be because there is already 0.2 hole/copper according to the formula. Its disappearance in the superconducting samples is consistent with the fact that the conductivity in layered cuprates is more confined to the CuO_2 layers.

The highest intensity peak at 559 cm^{-1} for $x = 0$ is shifted to higher frequency by 26 cm^{-1} in the whole range of substitution. Its intensity remains almost the same. Comparing with calculations and similar tetragonal system[10,20,21] this is an A_{2u} mode involving motion of O(3) along the *c*-axis. The increase of frequency is consistent with the decrease of Ba/Sr−O(3) bond length (see Table 2).

The phonon mode observed at 433 cm^{-1} ($x = 0$) decreases in intensity and disappears when the sample becomes superconducting. This indicates that it should involve motion of oxygen in the CuO_2 layer. By comparison, this can be assigned to the A_{2u} vibrational mode which involves motion of O(2) against Ca/Pr.

C. Raman Scattering. Raman spectra for a particular direction for three samples are shown in Figure 6. All three spectra are similar to that of its parent compound $TlBa_2CaCu_2O_7$.[23−25] Although the bulk samples contain a trace of impurities, the selected microcrystals examined do not present Raman features corresponding to impurities. Particularly, the Raman modes for the carbonates are expected to appear around 1000 cm^{-1}. The absence of such a feature suggests that all the peaks observed are intrinsic to the Tl-1212 phase.

Five totally different modes are observed in the present investigation. These are the modes that are commonly observed in Tl-1212 systems[10,23−25] and a structurally comparable system $YBa_2Cu_3O_{7-\delta}$.[21] For $x = 0$, only four modes at 128, 147, 294, and 511 cm^{-1} are observed. The most intense and highest frequency mode at 511 cm^{-1}, by analogy with $TlBa_2CaCu_2O_7$ and $YBa_2Cu_3O_{7-\delta}$ and also from the lattice dynamical cal-

(19) Mori, T.; Nakaoka, K.; Onari, S.; Arai, T. *Solid State Chem.* **1989**, *72*, 125.
(20) Kulkarni, A. D.; de Wetter, F. W.; Prade, J.; Schroder, U.; Kress, W. *Phys. Rev. B* **1990**, *41*, 6409.
(21) Thomsen, C.; Liu, R.; Bauer, M.; Wittlin, A.; Genzel, L.; Cardona, M.; Schonherr, E.; Bauhofer, W.; Konig, W. *Solid State Commun.* **1988**, *65*, 55.
(22) Mertelj, T.; Mihailovic, D.; Matacotta, F. C.; Liu, R. S.; Cooper, J. R.; Gameson, I.; Edwards, P. P. *Phys. Rev. B* **1993**, *47*, 12104.
(23) Huong, P. V.; Frison, J. C.; Chaminade, J. P. *Modern Aspects of Superconductivity*; Suryanarayanan, R., Eds.; IITT: Paris, 1989; p 149.
(24) Gasparov, L. V.; Kulakovskii, V. D.; Misochko, O. V.; Polyanskii, A. A.; Timofeev, V. B. *Physica C* **1989**, *160*, 147.
(25) Burns, G.; Crawford, M. K.; Dacol, F. H.; Herron, N. *Physica C* **1990**, *170*, 80.

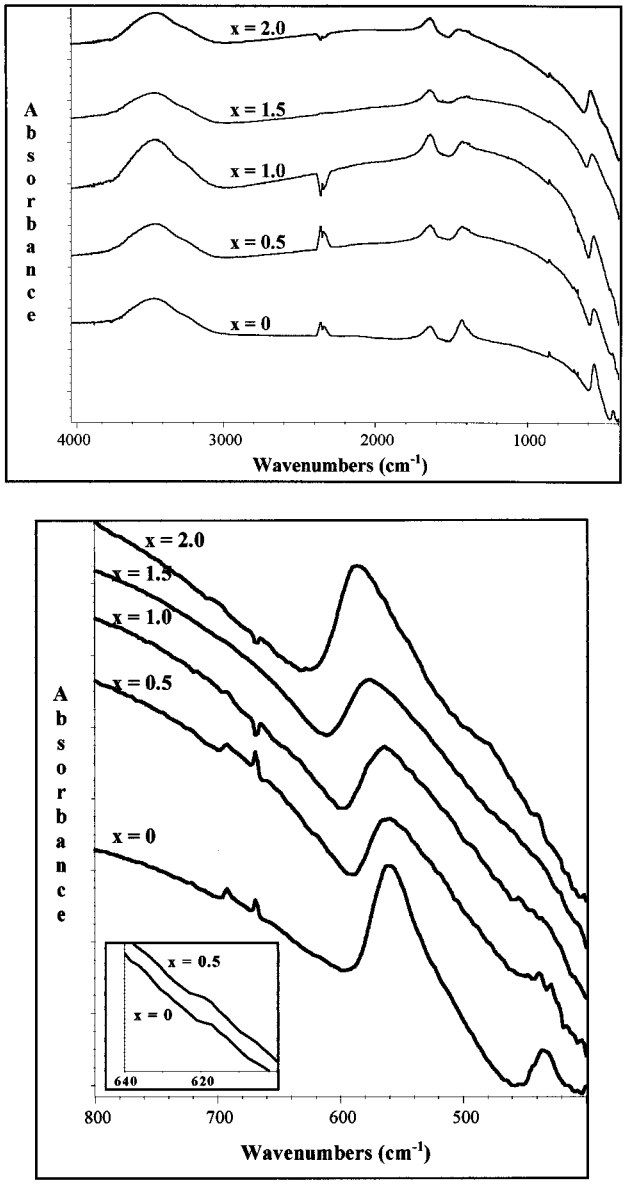

Figure 5. (a) Midinfrared absorption spectrum of $TlBa_{2-x}Sr_xCa_{0.4}Pr_{0.6}Cu_2O_{7-\delta}$ with various x. Shown in (b) is the detail spectrum. Inset shows the weak feature around 620 cm^{-1} in an expanded energy scale.

culations,[10,20] can be assigned to a symmetric stretching of apical oxygen O(1) atom along the *c*-axis. The position of this phonon mode shifts to higher frequency (~34 cm^{-1}) when x is increased to 2.0.

The next highest frequency mode is observed only in $x = 1.0$ and 2.0 at 414 and 412 cm^{-1}, respectively. These are A_{1g} modes that involve in-phase motion of O(2) along the *c*-axis. The phonon at 294 cm^{-1} for $x = 0$ can be ascribed to the B_{1g} mode. This is out-of-phase motion of O(2) along the *c*-axis. Its frequency and intensity decrease with an increase of x because of increased shielding by conducting holes.

The phonon frequency at 147 cm^{-1} in $x = 0$ increased by ~27 cm^{-1} over the entire range of substitution. This belongs to the A_{1g} vibration of Cu along the *c*-axis. The increase of frequency with x is consistent with the fact that the Cu−O(1) distance decreases (Table 2).

The lowest frequency mode for $x = 0$ is at 128.7 cm^{-1} and essentially involves the motion of the heavy atom such as Ba and Sr along the *c*-axis. This frequency

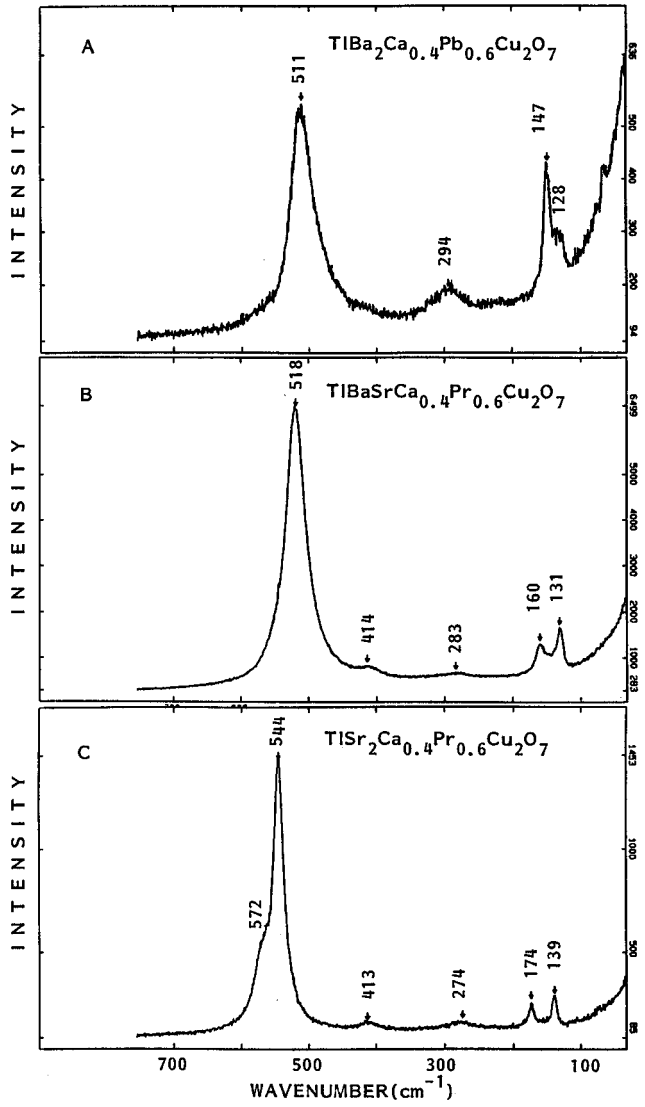

Figure 6. Room-temperature Raman spectra for a particular scattering geometry for $TlBa_{2-x}Sr_xCa_{0.4}Pr_{0.6}Cu_2O_{7-\delta}$.

increases with an increase of x which is consistent with the decrease of the Ba−O(3) bond length. In the case of $x = 2.0$, there is a shoulder at 572 cm^{-1}, which according to the calculations does not belong to the $TBa_2CaCu_2O_7$ tetragonal structure. Therefore, it may be due to possible lowering of symmetry induced by both smaller Sr^{2+} ions and disorder introduced by substitution of Ca^{2+} ions by Pr^{3+} ions.

3. Discussion

Consideration of thallium, oxygen deficiency, and the ratio of Ca/Pr (see Table 1), the estimated mean oxidation state of copper is +2.21, +2.25, +2.29 for $x = 0$, 1.0, and 2.0, respectively. These values do not vary so much to account for the observed insulator−superconductor transition. At this stage, analysis of various bond lengths are very instructive. It can be seen from Table 2 that the variation of the Tl−O(1) bond length with x is insignificant, whereas there is a large decrease in the Cu−O(1) distance. This indicates that the electrons are transferred from Cu:$3d_{z^2}$ band hybridized with $d_{x^2-y^2}$ and O_{2p} band to antibonding Tl:6s band. On the basis of this argument, one would expect that there should be an increase in the Tl−O(1) bond length with increase

of x. On the other hand, since the Ba^{2+} ions are substituted by smaller Sr^{2+} ions, we expect that Tl−O(1) bond length should decrease with an increase in x. Therefore, the insignificant change in the Tl−O(1) bond length results from these two competing effects. It is interesting to note that there is a large increase in the Cu−Cu distance with x. This seems to result from the large decrease of the Cu−O(1) distance. On the other hand, the Ca/Pr−O(2) distance shows only a small increase with x. This may be due to negligible change in the O(2)−Cu−O(2) bond angle in contrast to a decrease expected from the effect of chemical pressure.

The apical O(1) oxygen mode at 511 cm^{-1} observed in Raman scattering for $x = 0$ shows a large shift of frequency as x increases. In general, the change in phonon frequency reflects more the change in bond length. In the present case, since there is no marked change in the Tl−O(1) bond length (see Table 1) and that this apical O(1) oxygen which connects directly the charge reservoir (Tl) and CuO_2 layers, the large increase of frequency essentially indicates the charge transfer from Cu to Tl ions through apical oxygen. Similar evidence for charge transfer has already been reported.[10,21,26] In a system where there is no charge transfer, only a small shift ($\sim$4 cm^{-1}) of frequency is seen, for example in $La_{2-x}Sr_xCuO_4$.[27] It should be noticed that the change in frequency ($\sim$27 cm^{-1}) for a change in Cu−O bond length (0.323 Å) is smaller than that ($\sim$34 cm^{-1}) for a change of 0.01 Å in Tl−O(1) bond length. This strongly supports that there is a charge transfer from Cu to Tl ions. In contrast to the large frequency shift of the O(1) Raman-active mode, the large shift of the O(3) IR-active mode does not reflect the charge transfer between Tl and Cu, because the O(3) atom is sandwiched between Ba/Sr along the c-axis. Further, this mode is displaced perpendicular to the Tl−O(3) bond.

(26) Sacuto, A.; Julien, C.; Shchukin, V. A.; Perrin, C.; Mokhtari, M. *Phys. Rev. B* **1995**, *52*, 7619.

(27) Burns, G.; Chandrashekhar, G. V.; Dacol, F. H.; Shafer, M. W. *Solid State Commun.* **1988**, *68*, 67.

4. Conclusion

We have shown that substitution of smaller isovalent Sr^{2+} ions at the Ba^{2+} site in the $TlBa_2Ca_{0.4}Pr_{0.6}Cu_2O_{7-\delta}$ system leads to a transition from semiconductor to superconductor. Variation of the Tl−O(1) bond length, derived from a joint neutron/X-ray Rietveld refinement and the frequency change of Raman-active apical O(1) oxygen mode, suggests that there is a charge transfer from charge reservoir (Tl) to CuO_2 layers, which is suggested to be responsible for the semiconductor−superconductor transition observed in $TlBa_2Ca_{0.4}Pr_{0.6}Cu_2O_{7-\delta}$.

Acknowledgment. The authors would like to thank the Institut Max von Laue-Paul Langevin (ILL), Grenoble, France, for enabling the neutron diffraction experiment to be carried out. They also express their gratitude toward Dr. Emmanuelle Suard for her help in collecting the neutron data. Thanks are due to Dr. Marco Daturi (Istituto di chimica, Genova, Italy) for his help in the IR experiment and useful discussion.

CM970377C